


Outer Retinal Erosion and Outer Retinal Pinching at the Origin of Subretinal Fluid in Central Serous Chorioretinopathy



PAOLO FORTE, JENNIFER CATTANEO, SU-CHUN HUANG, PAOLO CORAZZA, SIMON MAGNIN, LORENZO MANGONI, STEFANO RANNO, CHRISTIAN CORDANO, ANTONIO POLITO, MASSIMO NICOLÒ, MICHELE IESTER, MARCO LUPIDI, CHIARA MARIA EANDI, AND FELICE CARDILLO PICCOLINO

- **PURPOSE:** To characterize early outer retinal changes at the site of origin of subretinal fluid (SRF) in central serous chorioretinopathy (CSCR). To investigate their pathophysiologic and clinical significance.
- **DESIGN:** Retrospective, nonconcurrent, multicenter cohort study.
- **SUBJECTS:** A total of 87 eyes of 87 patients with primary or recurrent CSCR (episode duration <4 months) and one or more fluorescein angiographic leaks.
- **METHODS:** In a series of cases of recently active CSCR, we analyzed changes occurring in the retina and subretinal space at the site of fluorescein leaks, taking into account similar finding already reported in the literature. Following the distinction of two basic findings definable as outer retinal erosion (ORE) and outer retinal pinching (ORP), we investigated associated clinical and morphological patterns. Volumetric quantification of SRF and pigment epithelial detachment (PED) was performed using artificial intelligence-enhanced algorithms (Discovery, RetinAI). Three-dimensional configurations of SRF volumes performed using custom scripts (MATLAB, MathWorks) provided complementary visualization of the retinal changes. Sixty patients had available follow-up of median 19 months. In these patients, time-to-event analysis with stratified log-rank test was performed to evaluate the development of foveal atrophy and posterior cystoid retinal degeneration (PCRD).

- **MAIN OUTCOME MEASURES:** SRF and PED volume. Development of foveal atrophy and PCRD.
- **RESULTS:** The cohort was divided according to the presence of ORE (43/87) and ORP (44/87) findings. ORP cases showed more frequent history of steroid use (40.9% vs 18.6%, $P = .011$), significantly higher SRF volumes (median 1763 vs 720 nL, $P = .0005$), more frequent PEDs (77.3% vs 46.9%, $P = .027$), and higher PED volumes (median 14.5 vs 0 nL, $P = .0002$). PCRD developed exclusively in ORP+ cases (7/28 eyes), with a median time to occurrence of 225 days, with no event in the ORE+ group (0/32 eyes). PCRD had an incidence of 0 versus 15.4 events per 100 person-years in ORE+ and ORP+ groups, and was associated with lower best-corrected visual acuity at the event (median = 0.3 vs 0.1 logMAR). No case developed foveal atrophy during the follow-up.
- **CONCLUSIONS:** ORE and ORP are two distinct disease pathways in CSCR. ORP cases, characterized by focal retinal pigment epithelium photoreceptor adherence and high-volume SRF, show significant risk of transition toward PCRD and limited visual loss. (Am J Ophthalmol 2026;286: 12–28. © 2026 Elsevier Inc. All rights are reserved, including those for text and data mining, AI training, and similar technologies.)

 Supplemental Material available at [AJO.com](https://www.ajon.com).
Accepted for publication February 15, 2026.

From the Fondazione Italiana Macula ETS, Genoa, Italy (P.F., J.C., L.M., M.N., M.L., C.M.E., F.C.P.); Jules-Gonin Eye Hospital, Fondation Asile des Aveugles, University of Lausanne, Switzerland (P.F., J.C., S.M., C.M.E.); IRCCS Ospedale Policlinico San Martino, Genoa, Italy (P.F., P.C., C.C., M.N., M.I.); DINOGLMI, University of Genoa, Italy (P.F., S.H., P.C., C.C., M.N., M.I.); Department of Ophthalmology, ASST Lariana, Sant'Anna Hospital, Como, Italy (J.C., S.R.); Department of Experimental and Clinical Medicine, Polytechnic University of Marche, Ancona, Italy (L.M., M.L.); IRCCS Sacro Cuore Don Calabria Hospital, Negrar, Verona, Italy (A.P.); Department of Surgical Sciences, University of Torino, Torino, Italy (C.M.E.)

Inquiries to Felice Cardillo Piccolino, Fondazione Italiana Macula ETS, Genoa, Italy; e-mail: felice.cardillopiccolino@gmail.com

Inquiries to Paolo Forte, University of Genova, Genova, Italy; e-mail: paolof97@gmail.com

CENTRAL SEROUS CHORIORETINOPATHY (CSCR) IS an idiopathic macular disorder characterized by a serous neurosensory retinal detachment where fluid originates from the choroid and reaches the subretinal space through a barrier defect of the retinal pigment epithelium (RPE). Its pathogenesis is not yet well defined and recognizes multiple risk factors that ultimately delineate a condition of choroidal overperfusion and choroidal veins dilation.¹⁻³ Although the literature of the last years has increasingly turned its attention to the posterior ocular compartments, the choroid and the sclera,⁴⁻⁶ investigation of outer retinal alterations remains essential to understand the severity of the clinical condition, to predict disease progression, and ultimately to plan therapeutic strategies.

The study of outer retinal and photoreceptor layer alterations has emerged as a significant focus in CSCR

research since the introduction of optical coherence tomography (OCT). Several studies documented the progressive changes occurring in the photoreceptor layer in chronic CSCR resulting in foveal atrophy and loss of visual acuity.^{7,8} Cystoid macular degeneration,⁹ later termed “posterior cystoid retinal degeneration” (PCRD),^{10,11} was also recognized as a complication not spontaneously resolving and associated with visual loss in advanced cases of disease.¹²

Numerous investigators have described early outer retinal modifications in CSCR, with particular emphasis on morphological features at the site of leaking points or pigment epithelium detachments (PEDs).¹³ However, a widely recognized classification of these findings and their prognostic significance have not been established. Various structural changes reported at the leakage sites include loss of the outer photoreceptor layer,^{14,15} suggesting disc erosion and displacement, and changes involving outer retina and RPE, described as “sagging,”¹³ “dragging,”¹⁶ “dipping,”^{13,16,17} with serous PED or subretinal fibrin,¹⁸ and “hyporeflexive subretinal lucency”¹⁹ within fibrinous material. Moreover, pathophysiology of these initial morphological changes and their relationship with subsequent disease evolution remain incompletely understood, limiting the ability in early stages to predict disease progression and contextually to make reliable therapeutic decisions.

We have designed a retrospective nonconcurrent study to systematically characterize early morphological patterns of CSCR and to investigate possible distinct disease trajectories linked to these patterns. The identification of peculiar morphological manifestations at the site of leaking points could provide biomarkers to identify the critical areas of chorioretinal exudation and potentially offer treatment guidance without the need for invasive imaging. In this investigation, we focused the attention on the possible correlation of early structural findings with the appearance of foveal atrophy and PCRD, as well as with the visual outcome. The study concerns the evolution of retinal lesions in patients who received an adequate treatment or observation during the follow-up period in centers that used to have a similar approach in managing the disease.

METHODS

In this multicenter, retrospective, nonconcurrent cohort study, we collected clinical records of patients diagnosed with CSCR between January 2019 and December 2024, corresponding to the baseline visit and, when applicable, to the follow-up visits, including those after half-dose photodynamic therapy (HD-PDT).²⁰ Patients were enrolled from 3 centers: Jules-Gonin Eye Hospital (University of Lausanne, Switzerland), IRCCS Hospital San Martino (University of Genoa, Italy), and Fondazione Italiana Macula ETS (Genoa, Italy). The study received approval from the

local Ethics Committee (CERVD: 2017–00493) and was performed in accordance with the principles outlined in the Declaration of Helsinki for research involving human subjects.

We included patients who at the first study visit had new symptoms within the last 4 months and were diagnosed with primary or recurrent simple CSCR according to the multimodal imaging-based classification (total area of RPE alterations ≤ 2 disc areas),²¹ with the presence of serous macular detachment and detectable focal dye leakage from the RPE on fluorescein angiography (FA). The exclusion of complex cases from the study was only functional to exclude advanced cases where early alterations of the outer retina at the site of leaking points might not be appreciable. From this perspective, the definition of simple CSCR was not applied with rigidity and arbitrarily extended to multifocal cases to be able to evaluate whether different outer retinal changes could be found at the site of different leaks in a same episode of CSCR. Diagnosis was also established based on pachychoroid detected with OCT²² and choroidal vascular hyperpermeability detected with indocyanine green angiography (ICGA).²³ Patients with the following conditions were excluded from the study: (1) any other chorioretinal or optic nerve disorder (ie, age-related macular degeneration); (2) relevant optic media opacities or insufficient fixation to allow high-quality imaging; (3) intraretinal fluid (IRF) or *bullous* CSCR phenotype at baseline; (4) annular RPE lesions or catenary forms typical of chronic CSCR;²⁴ (5) flat irregular PED with type 1 macular neovascularization detected by OCT angiography;²⁵ and (6) foveal atrophy at baseline according to a central foveal thickness cutoff equal $< 120 \mu\text{m}$.²⁶ In bilateral cases, only the eye with more recent symptoms was considered for the investigation. In all cases, treatment had followed the following criterion: HD-PDT guided by fluorescein and ICG angiography when spontaneous resolution had not occurred within 4 to 6 months, with a longer wait in case of subretinal fibrin.

• **DATA COLLECTION:** Clinical and demographic data were retrieved by independent readers for each institution (P.C., S.M., and F.C.P.). In addition to demographic records, we recorded the history of steroid use from the 6 months preceding the onset of the disease episode, then whether it was the first episode, and, in case of recurrence, the time interval since the last episode had occurred. From the clinical records, we also recorded best-corrected visual acuity (BCVA) using logMAR conversion and intraocular pressure (Goldmann tonometry). All patients had undergone structural OCT and OCT angiography (Spectralis HRA+OCT; Heidelberg Engineering) with a dense volumetric acquisition ($30^\circ \times 20^\circ$ or $20^\circ \times 20^\circ$ field, 97 sections, with automatic real-time function and enhanced depth imaging) mapping the entire subretinal fluid (SRF) volume. Radial OCT scans were analyzed to evaluate foveal involve-

ment and the relationship between the leakage sites and the central macula.

All patients had FA and ICGA available in the medical records (Spectralis HRA+OCT; Heidelberg Engineering) and OCT scans passing through the fluorescein angiographic leaking points. The OCT software enables direct multimodal cross-referencing of FA guide and corresponding OCT with closely spaced B-scans, ensuring accurate spatial localization.

- **FA GRADING:** Fluorescein leaks were classified according to the classic textbook of Shatz, Burton, Yannuzzi, and Rabb²⁷ by independent graders (P.F. and J.C.). Leaks begin as small “pinpoint” areas of hyperfluorescence at the level of the RPE in the arteriovenous phase.²⁷ Throughout the angiogram, fluorescein partially pools the space under the neurosensory retina in two patterns: (1) upward from a break in the RPE, forming a “mushroom,” “umbrella,” or “smokestack” appearance; (2) gradually increasing concentrically to form a spot resembling an “ink blot” with fuzzy margins. In cases of blot-type leaks, the leakage displays variable intensity, ranging from unusually “profuse” leaks to less pronounced amounts of fluorescence. Therefore, FA patterns were graded as “smokestack” or “blot-type” and additionally as “unifocal” or “multifocal,” with a subclassification of “profuse” for unusually intense leaks, using qualitative grading.

- **OCT GRADING:** All multimodal images were subsequently graded by the same independent graders (P.F. and J.C.). In addition to the presence of serous PED, which represents a well-established possible location of leak site,^{13,28} graders conducted comprehensive morphological analysis of outer retinal structures on OCT B-scans passing through FA-confirmed focal leaks.

The evaluation protocol documented structural abnormalities of the outer retina in the macular area with serous detachment. Graders particularly assessed the continuity and integrity of the outer photoreceptor layer at the site of the leaking point of the RPE, with documentation of focal interruptions along an otherwise thickened outer photoreceptor layer. Graders also evaluated the localization and extent of subretinal fibrin,^{17,29} which was defined as hyper-reflective material above the RPE. Morphological changes of the outer retina and RPE in correspondence with the fibrinous deposits were evaluated. Analysis of these morphological features across the entire cohort revealed two distinct outer retinal configurations at leakage sites, which are subsequently defined and characterized in the “Results” section.

Records of all cases related to the follow-up visits were analyzed, and the date of any appearance of foveal atrophy²⁶ or PCRD,¹⁰ defined by the presence of optically empty spaces of IRF at the posterior pole or other structural retinal changes, was recorded. An additional blinded grader (F.C.P.) was involved in case of inter-graders’ discordance.

- **RENDERING OF SRF VOLUME:** Three-dimensional reconstruction and rendering of SRF volume were performed using custom scripts (S.H.) developed in MATLAB (v. 2024b; MathWorks). The OCT volumetric scan and corresponding segmentation boundaries—internal limiting membrane (ILM) and Bruch’s membrane—were exported in “.raw” format. Preprocessing included A-scan-wise intensity normalization to standardize brightness levels across all B-scans. The retinal region was defined as the area between the internal limiting membrane and Bruch’s membrane in each scan. A binary mask was then applied, with a threshold set at 0.1% of the maximum intensity within the retinal area. The threshold was empirically determined to optimize sensitivity to low-intensity SRF signals while minimizing noise artifacts. Voxels located within the retinal boundaries but excluded by the mask were identified as SRF volume. For volumetric rendering, the spatial coordinates of the SRF voxels were mapped to the original OCT coordinate space. These coordinates were subsequently triangulated into tetrahedra using the MyRobustCrust algorithm. The SRF volume was visualized by rendering the isosurface of the resulting tetrahedral mesh, enabling systematic analysis of distinct SRF morphological configurations. Two independent graders (P.F. and J.C.) performed comprehensive evaluation of SRF volume maps to identify and classify morphological characteristics that would subsequently inform the primary study findings.

- **ARTIFICIAL INTELLIGENCE-ENHANCED FLUID QUANTIFICATION:** After anonymization, OCT volumes were analyzed using the Discovery platform (Discovery OCT Fluid and Biomarker Detector, RetinAI AG) providing automated quantification of retinal and choroidal layers thickness and volumes. This software is based on a convolutional neural network architecture and was trained in a supervised manner.³⁰ Specifically, the artificial intelligence (AI)-assisted volumetric analysis provides quantification of SRF and PED volumes measured in nanoliters, in analogy to previous studies.^{31,32} When an error in automated thickness or volume was present, manual editing was performed (C.M.E.).

- **STATISTICAL ANALYSIS:** Statistical analyses were performed using R software (version 4.3.3). Column graphs and survival curves were created using GraphPad Prism software (version 10.0.0). Main outcome measures were (1) AI-enhanced volumetric quantification of SRF and PED between morphological groups identified in the study; and (2) development of adverse anatomic outcomes (foveal atrophy and PCRD) during the follow-up window. Quantification of SRF and PED volumes was the primary outcome, whereas follow-up analysis was considered exploratory and hypothesis-generating.

Continuous variables are presented as median and interquartile range (IQR), and nonparametric tests were applied. The Mann–Whitney *U* test was used for continuous

variables, and categorical variables were compared using the chi-square test. Time-to-event analysis used Kaplan–Meier estimators with the log-rank test for comparative analysis between morphological groups identified during the study, with observation censored at the date of onset of PCRD or foveal atrophy, or upon the last follow-up for unaffected eyes. For descriptive purposes, patients who developed these events continued to be observed throughout the available follow-up period, with documentation of additional treatments and final visual acuity. Event-free survival probabilities with 95% CIs were calculated at landmark time points of 6, 12, and 24 months. The ratio between the number of adverse events and the total observation time was used as an estimate of the incidence rate per 100 person-years. For stratified analyses by treatment status, patients were categorized based on whether they received HD-PDT or observation during the follow-up period, and event rates were calculated for each subgroup. *P* values < .05 were considered statistically significant.

RESULTS

• **IDENTIFICATION OF TWO DISTINCT OUTER RETINAL PATTERNS:** B-scan OCT and 3-dimensional rendering analysis of SRF volume revealed two distinct mutually exclusive morphological configurations of the outer retinal changes at the leakage sites.

- **Outer Retinal Erosion (ORE):** This pattern was characterized by a notch-shaped erosion, or a broader loss of tissue, along an otherwise thickened outer photoreceptor layer within the macular detachment, creating a "tooth loss" appearance. The volume of SRF in cases with ORE displays a conventional dome configuration.
- **Outer Retinal Pinching (ORP):** this pattern was defined by the presence of focal adherence or hyperreflective connecting material, presumed to be fibrin, between the RPE and the outer photoreceptor layer within the serous macular detachment. Traction on both sides of the subretinal space creates a characteristic "pinching" effect on the outer retina and the RPE, mainly appreciable on the retinal side. Consequently, the volume of SRF displays an eccentric toroidal or doughnut-like configuration.

The cohort was divided between these two patterns, with ORE identified in 43 cases (49.4%) and ORP in 44 cases (50.6%). Representative examples of the multimodal imaging and corresponding OCT morphological features are illustrated in [Figure 1](#). The characteristic differences in SRF volume configuration between ORE and ORP patterns are visualized through 3-dimensional rendering in [Figure 2](#).

• **DEMOGRAPHICAL AND CLINICAL FEATURES:** The study cohort comprised 87 eyes of 87 patients with a predominant

male representation of 74.7%. The median age of patients was 46 years with an IQR of 41 to 51 years and a total range spanning from 30 to 76 years. First episodes accounted for 29 of 87 cases (33.3%), and 58 of 87 (66.6%) were recurrences. Recurrent cases had a median time from first episode of 2 years (IQR, 1-4; min-max: 1-13). Steroid-related cases represented 26 of 87 (29.9%) of the sample. Comprehensive demographics and baseline characteristics are detailed in [Table 1](#).

• **PATTERN-SPECIFIC MORPHOLOGICAL CHARACTERISTICS:** Among ORE cases, a notch-shaped erosion of the outer segments of photoreceptors ([Figure 3, A](#)) was present in 32 cases representing 74.4% of this group, whereas a broader erosion ([Figure 3, B](#)) was observed in 11 cases representing 25.6%. These lesions were differentiated by photoreceptor atrophy due to long-lasting SRF for the clear demarcation of the tissue loss in the context of a thickened outer photoreceptor layer. Thinning of the outer nuclear layer could be seen in correspondence with the outer segment loss.

The focal subretinal adherence characteristic of ORP cases demonstrated several distinct morphological presentations. The area of adherence and traction corresponded with a subretinal fibrin bridge with occasional hyporeflective subretinal lucency, or, less frequently, to a "clepsydra" appearance, in which the posterior displacement of the outer retina without interposition of fibrin was juxtaposed with a pointed serous RPE detachment. A fibrin bridge between the outer retina and RPE ([Figure 3, D](#)) was identified in 38 cases representing 86.3% of the ORP group, indicating the peculiar role of fibrinous material in establishing retinal-RPE adherence and traction. A concurrent hyporeflective lucency ([Figure 3, E](#)) was evident in 13 cases representing 29.5% of the ORP group and was observed in all cases in the subretinal compartment within areas of massive fibrin deposition above the RPE plane. Six of the ORP cases (13.6%) presented with a clepsydra appearance ([Figure 3, C](#)).

• **ORE VERSUS ORP COMPARISON:** Comparative analysis between ORE (*n* = 43) and ORP (*n* = 44) groups revealed significant morphological and volumetric differences ([Table 2](#)). The groups were well matched regarding demographic and clinical parameters, with no significant differences in age (median: 46.0 vs 45.5 years, *P* = .677), proportion of first episodes (32.6% vs 34.1%, *P* = .877), or baseline BCVA (median: 0.1 vs 0.2 logMAR, *P* = .777). The prevalence of steroid-related episodes (18.6% vs 40.9%, *P* = .011) was markedly higher in the ORP group.

The proportion of cases with detectable PED was significantly higher in the ORP group (77.3% vs 46.9%, *P* = .027). In contrast, volumetric measurements revealed profound differences between patterns. ORP cases exhibited significantly higher median SRF volumes (1763 nL

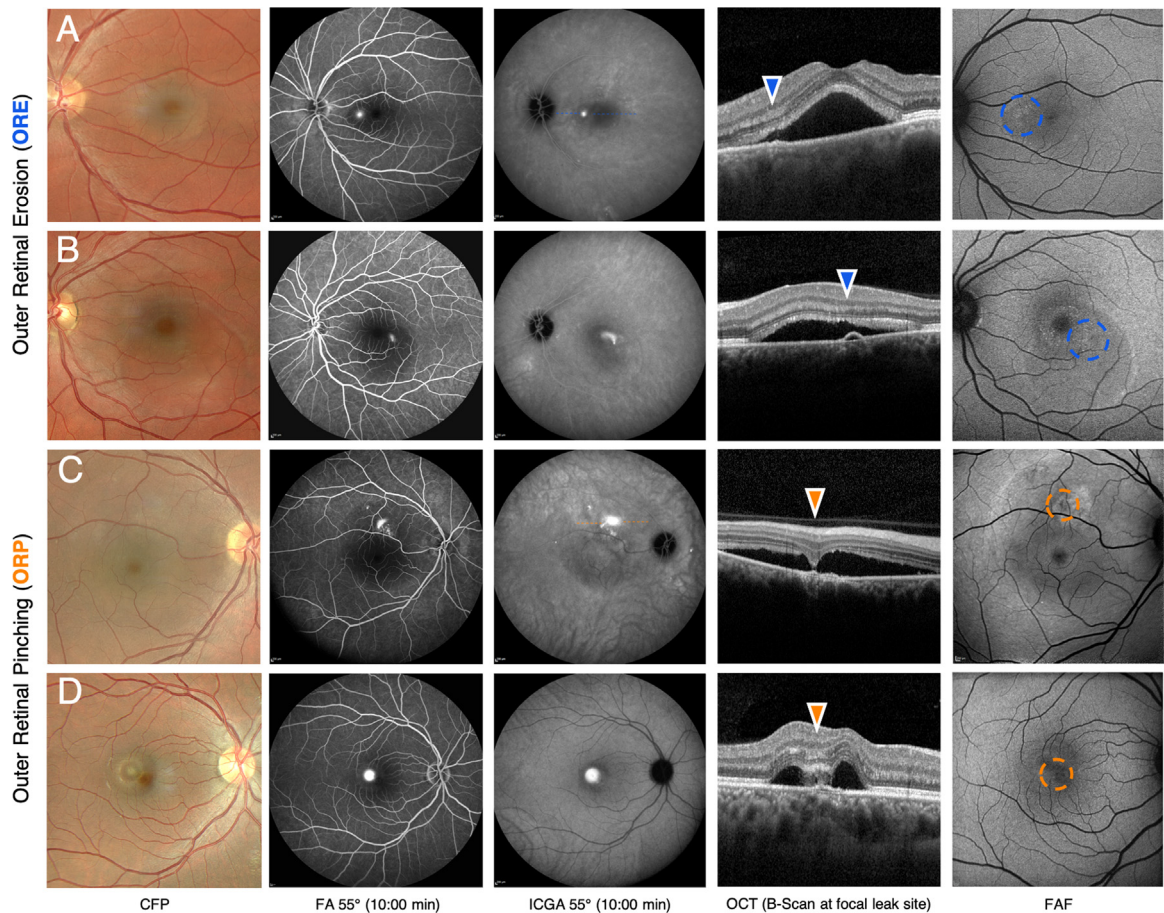


FIGURE 1. Representative examples of the multimodal imaging and corresponding optical coherence tomography (OCT) patterns of the outer retina. **A** and **B.** Outer retinal erosion (ORE) cases showing focal notch-shaped erosion (**A**) or broader (**B**) photoreceptor thinning overlying pigment epithelium detachment (PED) (*blue arrowheads*) with mild fluorescein angiography (FA) leakage and focal hyper-autofluorescence due to window effect from photoreceptor layer thinning. **C.** Outer retinal pinching (ORP; *orange arrowhead*) case with smoke-stack FA leak and clepsydra sign (ie, posterior displacement of the outer retina without clear interposition of fibrin). **D.** ORP case with blot-type leak, ring-shaped subretinal exudates, fibrin bridge, and hyporefective lucency. The leak intensity is more pronounced on indocyanine green angiogram, congruous with greater degree of vascular hyperpermeability. Fundus autofluorescence reveals a focal area of nonfluorescence corresponding to the site of the retinal pigment epithelium (RPE) barrier defect.

[IQR, 957-3288] vs 720 nL [IQR, 395-1197], $P = .0005$) compared with ORE cases. Likewise, median PED volumes were substantially greater in ORP cases compared with ORE cases (14.5 nL [IQR, 4-41] vs 0 nL [IQR, 0-4], $P = .0002$). The volumetric differences of SRF and PED between ORE and ORP cases are graphically represented in [Figure 4](#), **A** and **B**.

Subgroup analysis restricted to unifocal leaks ($n = 38$ per group) confirmed significant volumetric differences between the two patterns. Median SRF volume was 715 nL (IQR, 361-1287) in ORE versus 1668 nL (IQR, 673-3093) in ORP (Mann-Whitney U test, $P = .0013$). Median PED volume was 0 nL (IQR, 0-4) in ORE versus 12.5 nL (IQR, 2-32) in ORP ($P = .00019$). Multifocal cases (ORE $n = 5$, ORP $n = 6$) showed median SRF volumes of 481 nL and 1205 nL, respectively, indicating that multifocality per se

was not associated with higher total fluid volumes. Representative examples from the subgroup analysis restricted to unifocal leaks with volumes near group medians are shown in [Figure 4](#), **C** and **D**.

• **ANGIOGRAPHIC AND AUTOFLUORESCENCE FEATURES:** FA pattern analysis showed blot-type leaks in 76 of 87 patients (87.4%) and smoke-stack leaks in 11 of 87 patients (12.6%). Profuse leak intensity was observed in 16 of 87 patients (18.3%). No significant differences were observed in fluorescein leak type between the ORE and ORP groups, with blot-type leaks predominating in both groups (88.4% vs 86.4%, $P = .774$) and similar distribution of smoke-stack pattern (11.6% vs 13.6%). Smokestack leaks characterized cases with the clepsydra sign in the ORP group and broader erosion in the ORE group ([Table 2](#)).

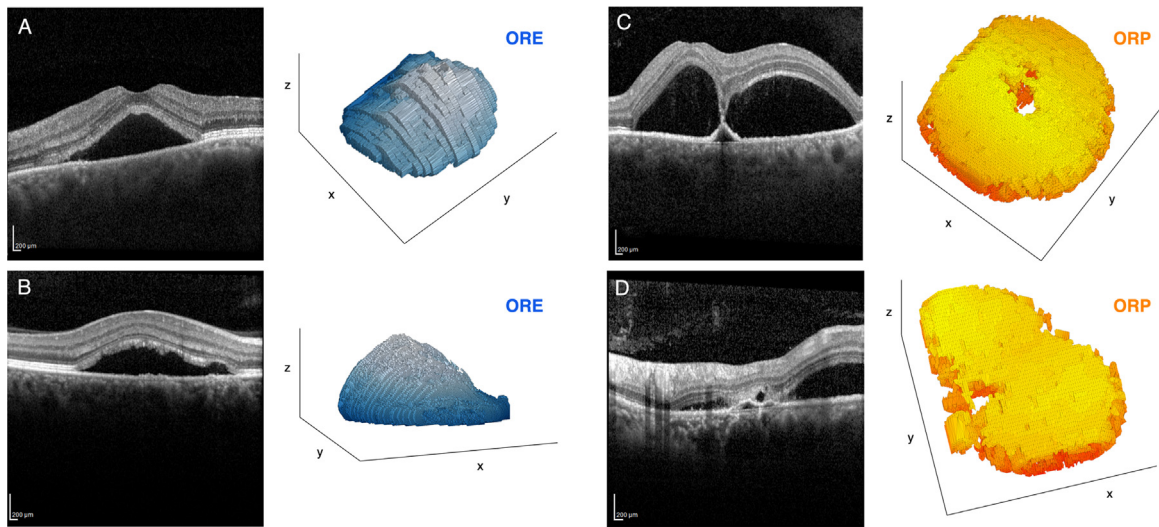


FIGURE 2. Three-dimensional rendering of subretinal fluid (SRF) volume configurations demonstrating two distinct morphological outer retinal patterns in central serous chorioretinopathy (CSCR). A and B. ORE cases show conventional dome or conical SRF volume configuration characterized by focal erosion of the outer photoreceptor layer while maintaining separation between retinal and RPE layers within the serous neuroretinal detachment. C and D. ORP cases exhibit characteristic toroidal or doughnut-shaped SRF morphology resulting from focal contact and adherence between the RPE and outer photoreceptor layer, creating a distinctive "pinching" effect that constrains SRF flow around a focal adherence point. ORE = outer retinal erosion.

TABLE 1. Demographics and Baseline Characteristics of 87 Eyes of 87 Patients

Variable	N/Total (%)
Male gender	65 (74.7%)
Steroid correlation	26 (29.9%)
Episode: First onset	29 (33.3%)
Episode: Recurrence	58 (66.6%)
FA Pattern	
Blot-type leak	76 (87.4%)
Smoke-stack leak	11 (12.6%)
Multifocal leaks	12 (13.7%)
Profuse intensity	16 (18.3%)
OCT-Associated Features	
ORE – Tooth Loss Sign	43 (49.4%)
Focal notch	32 (36.8%)
Broader erosion	11 (12.6%)
ORP	44 (50.6%)
Fibrin bridge	38 (43.7%)
Hyporeflective lucency	13 (14.9%)
Clepsydra sign	6 (6.9%)
Continuous Variables	Median (IQR) [min-max]
Age, years	46 (41-51) [30-76]
Symptoms onset, years (in 58 recurrent cases)	2 (1-4) [1-13]

FA = fluorescein angiography; IQR = interquartile range; OCT = optical coherence tomography; ORE = outer retinal erosion; ORP = outer retinal pinching.

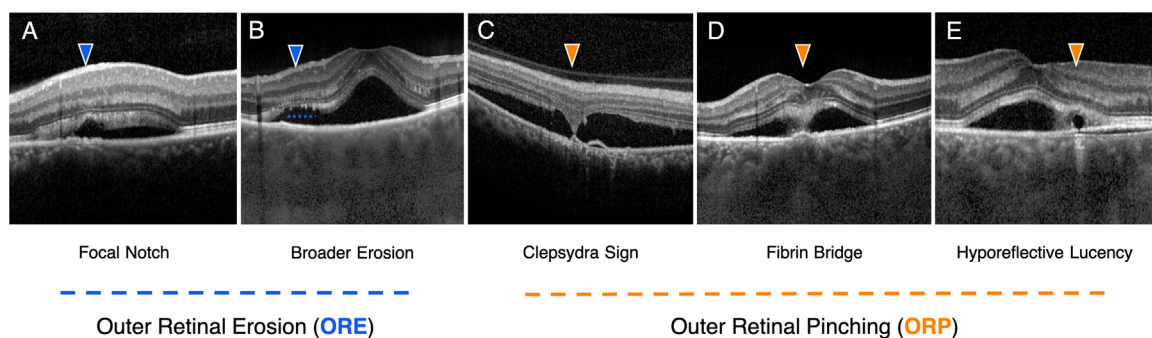


FIGURE 3. Representative examples of OCT morphological grading adopted in the study. Blue arrowheads indicate ORE patterns; orange arrowheads indicate ORP patterns. A. Notch-shaped erosion: discrete interruption along an otherwise thickened outer photoreceptor layer. B. Broader erosion: broader confluent thinning of the outer photoreceptor layer. C. Clepsydra sign: posterior displacement of the outer retina indicating subclinical fibrinous adhesion. D. Subretinal fibrin bridge: well-defined proteinaceous material bridging the RPE and outer photoreceptor layer. E. Hyporeflective subretinal lucency: hyporeflective area within fibrinous deposits above the plane of the RPE.

TABLE 2. Comparison Between Outer Retinal Erosion and Outer Retinal Pinching Groups

Variable	ORE (N = 43)	ORP (N = 44)	P Value
First episode, n (%)	14 (32.6%)	15 (34.1%)	.877
Steroid correlation, n (%)	8 (18.6%)	18 (40.9%)	.011*
PED presence, n (%)	20 (46.9%)	34 (77.3%)	.027*
Leak type on FA, n (%)			.774
- Blot-type	38 (88.4%)	38 (84.6%)	
- Some-stack	5 (11.6%)	6 (13.6%)	
Leak number of FA, n (%)			.306
Unifocal	37 (86.0%)	38 (86.4%)	
Multifocal	6 (14.0%)	6 (13.6%)	
Profuse intensity, n (%)	3 (6.9%)	13 (29.5%)	.003*
Age, years	46 (42-52)	45.5 (41-50)	.677
BCVA (logMAR)	0.1 (0-0.3)	0.2 (0.1-0.3)	.777
IOP (mmHg)	13 (10-14)	13 (11-14)	.966
SRF volume (nL)	720 (395-1197)	1763 (957-3288)	.0005*
PED volume (nL)	0 (0-4)	14.5 (4-41)	.0002*

Continuous variables were analyzed using Mann–Whitney *U* test. Categorical variables were analyzed using chi-square test.

BCVA = best-corrected visual acuity; FA = fluorescence angiography; IOP = intraocular pressure; ORE = outer retinal erosion; ORP = outer retinal pinching; PED = pigment epithelial detachment; SRF = subretinal fluid.

Leaks were predominantly unifocal in both groups (86.0% vs 86.4%), with comparable multifocal presentation (14.0% vs 13.6%, $P = .306$). However, profuse leak intensity was significantly more frequent in ORP cases (6.9% vs 29.5%, $P = .003$), aligning with quantitative volumetric quantification.

In cases with multifocal FA leaks, ORE and ORP were not present in the same eyes. Each leakage site within individual patients demonstrated the same morphological pattern on OCT either exclusively ORE or exclusively ORP; an example is shown in Figure 5. In multifocal ORE cases, the photoreceptor's displacement was not equally pronounced at all fluorescein leak sites; this heterogeneity is consistent with the concept that not all angiographically detected leaks contribute equally to SRF accumulation.³³

On FAF, in case of ORE, the zonal loss of photoreceptors outer segments was slightly hyperfluorescent (Figure 1) due to the increased transmission of the RPE autofluorescence signal of the underlying RPE (G. Staurenghi, personal communication). Instead, in case of ORP, FAF usually revealed a focal area of nonfluorescence corresponding to the site of the RPE barrier defect,³⁴ more obvious in cases of profuse leakage.

• **FOLLOW-UP EVALUATION:** Sixty patients, 32 with ORE and 28 with ORP, had available follow-up records of a median of 19 months. No crossover between ORE and ORP patterns was observed during the follow-up period. Thirty-two of these patients (53.3%) were treated with PDT during the observation period, including 19 (59.4%) from the

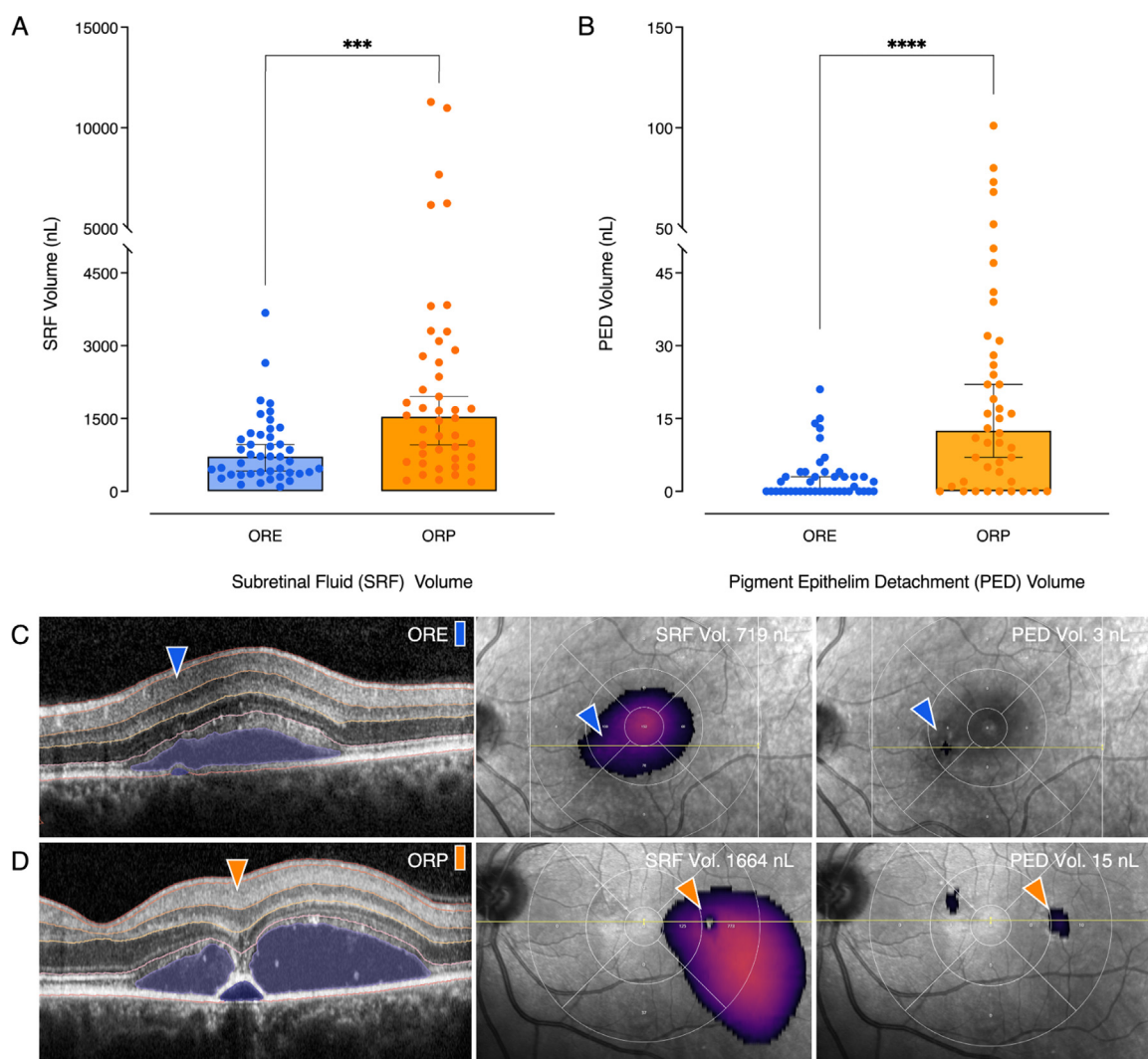


FIGURE 4. Comparison of SRF and pigment epithelial detachment (PED) volumes between ORE and ORP groups. **A** and **B.** Scatter plots with segmented y-axis demonstrate significantly higher volumes in ORP cases for both SRF ($P = .0005$) and PED ($P = .0002$) volumes, reflecting the association between ORP pattern and more profound choroidal hyperpermeability. **C** and **D.** Representative examples from the subgroup analysis restricted to unifocal leaks with volumes near group medians. B-scans show the segmentation boundaries with corresponding SRF and PED volume maps. Note in ORP case (*orange arrowhead*): toroidal SRF configuration with the adherence site as epicenter of subretinal exudation. ORE = outer retinal erosion; ORP = outer retinal pinching.

ORE group and 13 (46.6%) from the ORP group. HD-PDT was performed at a median of 41 days (IQR, 21-78) from baseline evaluation. Treatment resulted in complete SRF reabsorption in all cases of both groups; however, 7 eyes with ORP developed PCRD (Table 3). Final foveal atrophy was not detected in any case. Consequently, time-to-event analysis using Kaplan–Meier estimators demonstrated significantly higher IRF-free survival in ORE compared with ORP patients, as presented in Figure 6 and Table 4. The 24-month landmark IRF-free survival rate was 100% for ORE patients versus 72.1% for ORP patients (95% CI, 56.3-89.2), with log-rank test confirming statistical significance (chi-square = 7.95, $P = .005$). All 7 IRF events occurred exclusively in the ORP group ($n = 28$), with none observed

in the ORE group ($n = 32$) during the entire observation period.

Among the 7 patients who developed PCRD, the median time to IRF development was 225 days (IQR, 183-295) from baseline for all events. Five of these cases were untreated, and two had received HD-PDT approximately 3 months earlier. In the latter, PCRD was detected at the first follow-up visit after treatment, approximately 9 months after baseline in 1 month and 3 months after baseline in the other. In the two patients in whom PCRD developed after treatment, the PDT spots corresponded spatially to the subsequent PCRD development. Among untreated patients, the median time to IRF development was 237 days (IQR, 186-304). The stratified log-rank test, which accounts for

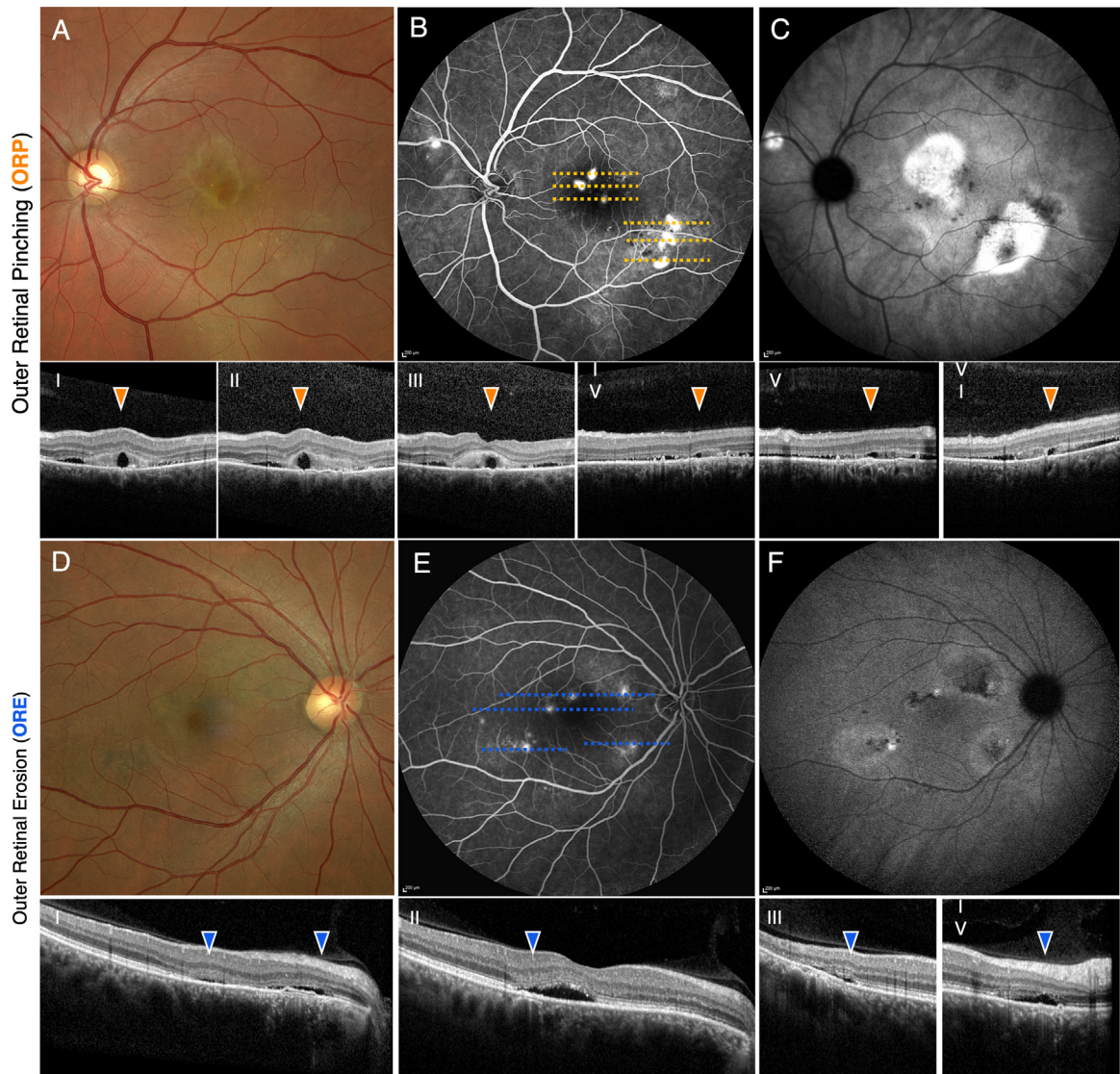


FIGURE 5. Multifocal leakage patterns demonstrating outer retinal morphological consistency within individual patients. *Top rows:* ORP case with multifocal leaks (ID2). A. Color fundus photography (CFP) reveals multifocal ring-shaped exudates and translucent areas corresponding to fibrin deposition, with turbid SRF. B. FA shows multiple active blot-type leaks (profuse specification). C. Late-phase indocyanine green angiography (ICGA) demonstrates intense hyperpermeability and dye coalescence through the leak sites. I-VI. Corresponding OCT B-scans reveal multifocal hyporeflective subretinal lucency at the RPE plane, with ORP pattern thus present simultaneously at all leakage sites (*orange arrowhead*). *Bottom rows:* ORE case with multifocal leaks. D. CFP shows multifocal neurosensory retinal detachments without visible fibrin deposition. E. FA demonstrates multifocal leaks with modest intensity. F. Late-phase ICGA shows mild hyperpermeability, heterogeneous among the leak points identified on FA. I-IV. Corresponding OCT B-scans demonstrate multiple notch-shaped ORE areas (*blue arrowheads*); ORE features are not equally pronounced at all points since not all angiographically detected leaks contribute equally to SRF accumulation.

treatment status as a stratification factor, confirmed a significant difference in IRF-free survival between the ORE and ORP groups (chi-square = 8.96, $P = .003$). This finding suggests that the observed survival difference between morphological patterns persists even after accounting for treatment effect. Incidence rate analysis revealed 0 events per 100 person-years in the ORE group compared with 15.4 events per 100 person-years in the ORP group. In the 7 cases

complicated with PCRD, IRF was associated with serous detachment of the adjacent neuroepithelium that involved the fovea in 4 cases.

- **FEATURES OF CASES DEVELOPING PCRD:** All 7 patients who developed IRF were recurrent CSCR cases, with blot-type leakage on FA and presence of subretinal fibrin. De-

TABLE 3. Posterior Cystoid Retinal Degeneration–Free Survival Analysis According to Kaplan–Meier Estimates in 60 Eyes of 60 Patients With Available Follow-up and Treatment With Half-dose Photodynamic Therapy

Events	ORE (N = 32)	ORP (N = 28)	Overall (N = 60)
Median follow-up, days (IQR)	766 (440-1206)	489 (254-780)	570 (308-1028)
PCRD development, n (%)	0 (0.0%)	7 (25.0%)	7 (11.7%)
Median time to event, d (IQR)	Not reached	225 (183-295)	-
Log-rank test, chi-square	-	-	8.96
P value	-	-	.003*
Treatment Information			
Treated patients, n (%)	19 (59.4%)	13 (46.4%)	32 (53.3%)
Median time to HD-PDT, days (IQR)	31 (21-113)	32 (22-48)	41 (21-78)
PCRD in untreated patients, n (%)	0/13 (0.0%)	5/15 (33.3%)	5/29 (17.9%)
PCRD in treated patients, n (%)	0/19 (0.0%)	2/13 (15.4%)	2/31 (6.3%)
Stratified log-rank by treatment, chi-square	-	-	7.95
P value	-	-	.005*
PCRD-free Survival Landmark Analysis			
6-months (95% CI)	100%	96.4% (76.5-99.5%)	98.3% (88.8-99.8%)
12-months (95% CI)	100%	77.3% (61.0-91.8%)	89.3% (79.9-96.3%)
24-months (95% CI)	100%	72.1% (56.3-89.2%)	89.5% (77.8-95.1%)
Incidence rate (per 100 person-y)	0.0	15.4	5.8

HD-PDT = half-dose photodynamic therapy; IQR = interquartile range; ORE = outer retinal erosion; ORP = outer retinal pinching; PCRD = posterior cystoid retinal degeneration.

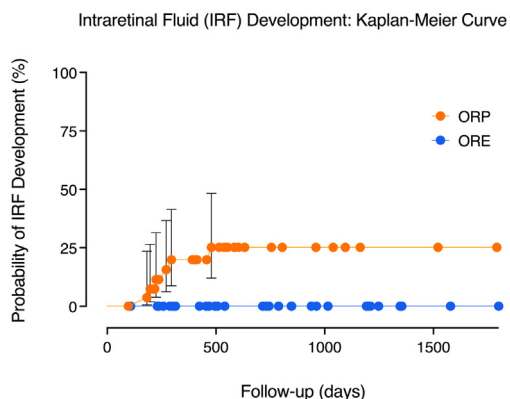


FIGURE 6. Kaplan–Meier survival curves for intraretinal fluid (IRF) development in the phenotype of posterior cystoid retinal degeneration (PCRD) stratified by ORE and ORP cases. All IRF events occurred in ORP group (7/28 patients) with median time to development of 225 days, whereas no events were observed in ORE cases (0/32 patients). Log-rank test P value = .003. ORE = outer retinal erosion; ORP = outer retinal pinching.

tailed individual patient characteristics are reported in Table 4.

In all PCRD cases, cystoid cavities corresponded to the area of previous ORP and were predominantly located in the outer nuclear layer. Cysts of smaller size were also present in the inner nuclear layer. The largest optically empty cavities were directly adjacent to the retinal-RPE

adhesion site and arranged with other smaller cysts in a connected pattern. Foveal involvement by cystic cavities (within central 1.50 mm) was observed in 2 of 7 cases. All cases demonstrated interruption of the external limiting membrane and atrophy of the RPE in the area of chorioretinal adherence. In the same area, fundus autofluorescence showed hypo or absent fluorescence. The topographic distribution of PCRD cases was variously located at the posterior pole, as illustrated in Figure 7. Representative examples of follow-up evaluations of ORE and ORP cases are shown in Figure 8.

Among ORP cases, patients who developed IRF demonstrated significantly worse visual acuity at PCRD onset compared with those without IRF development, with a median logMAR BCVA of 0.3 (IQR, 0.1-0.4) versus 0.1 (IQR, 0.0-0.1), respectively (P = .003).

Extended follow-up of PCRD cases (median, 2.3 years; range, 0.5-6.3 years) showed visual stabilization or improvement in 6 of 7 cases, with persistent intraretinal fluid in 6 cases and complete SRF resolution in 5 cases at final evaluation. PDT treatments were required in 6 cases. Foveal involvement by persistent intraretinal fluid occurred in 2 cases, and no patient developed foveal atrophy during the extended follow-up period (Table 4).

DISCUSSION

This study describes two distinct early patterns of retinal changes that can be observed at the site of origin of SRF

TABLE 4. Clinical and Imaging Features of Seven Outer Retinal Pinching Patients Who Developed Posterior Cystoid Retinal Degeneration

ID	Gender and Age (y)	Steroid Correlation	Localization (x, y; μm)	FA Leak Type	Fibrin Bridge	SRF Volume (nL)	PED Volume (nL)	PCRD After HD-PDT	PCRD Development (mo)	Baseline BCVA (logMAR)	PCRD Detection BCVA (logMAR)	Further Follow-up (y)	Additional Treatments	Final BCVA (logMAR)
ID1	M, 75	No	Extra-foveal (-735, 826)	Blot-type	Present	706	6	No	6.6	0	0	6.3	2 HD-PDT	0.2
ID2	M, 35	Yes	Foveal (-601, 404)	Blot-type Multifocal	Present + Lucency	1137	26	No	6	0.2	0.4	0.8	1 HD-PDT	0.4
ID3	M, 65	No	Extra-foveal (97, 2128)	Blot-type	Present	913	24	No	7.5	0	0.1	2.3	1 HD-PDT	0.1
ID4	M, 35	Yes	Foveal (479, 544)	Blot-type	Present	223	13	No	16.0	0.4	0.5	2.1	2 HD-PDT	0.1
ID5	F, 56	Yes	Extra-foveal (-1034, 711)	Blot-type	Present	673	16	No	9.0	0.1	0.2	0.5	-	0.2
ID6	M, 44	No	Extra-foveal (2847, 2341)	Blot-type	Present	3833	7	Yes	9.8	0	0.3	4.1	2 HD-PDT	0
ID7	M, 59	Yes	Extra-foveal (2540, 1239)	Blot-type	Present + Lucency	2652	50	Yes	3.3	0.1	0.3	3.2	2 HD-PDT	0.1

All cases were recurrent episodes displaying blot-type leak on fluorescein angiogram and ORP on OCT at baseline.

BCVA = best-corrected visual acuity; FA = fluorescein angiography; ID = patient identifier; HD-PDT = half-dose photodynamic therapy; PCRD = posterior cystoid retinal degeneration; PED = pigment epithelium detachment; SRF = subretinal fluid.

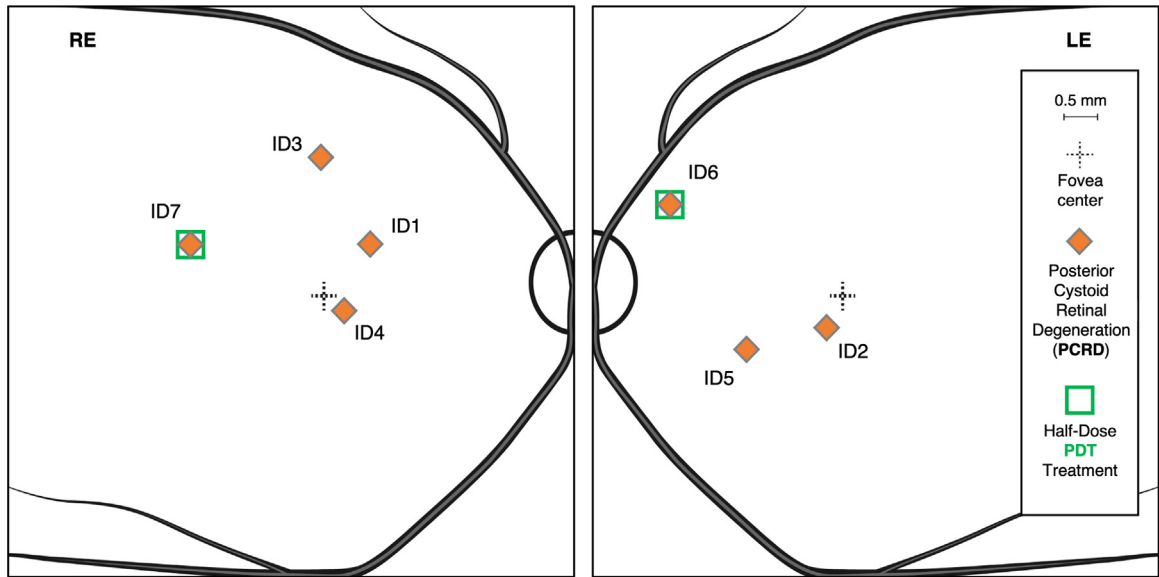


FIGURE 7. Topographic localization of PCRD cases in relation to fovea center and half-dose photodynamic therapy (HD-PDT) treatment status. Bilateral fundus map demonstrates spatial localization of 7 PCRD cases (gray diamonds) across the posterior pole, with 2 cases receiving half-dose PDT treatment (green squares). All PCRD cases developed exclusively in patients with ORP group, with variable distance from foveal center.

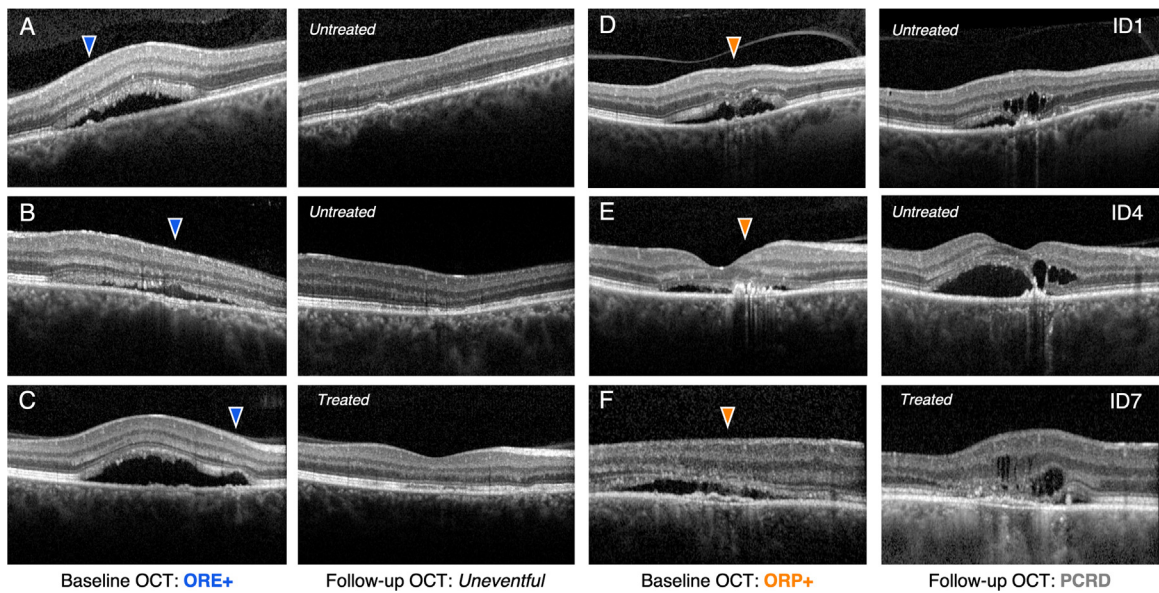


FIGURE 8. Example cases of follow-up evaluation in ORE cases and ORP untreated and treated cases at IRF development (ID1, ID4 and ID7). A to C. ORE cases with “tooth loss sign” demonstrating favorable anatomic outcomes. The residual focal thinning of the outer nuclear layer after SRF resolution likely represents photoreceptor misalignment and erosion resulting from the mechanical action of fluid flow during the active phase. D to F. ORP cases showing baseline focal adherence progressing to intraretinal cyst formation. Strong spatial correlation is observed between the original pinching sites and subsequent cystoid cavity development, with ID7 receiving half-dose PDT treatment. The anatomic progression demonstrates how focal chorioretinal adherence facilitates direct communication between choroidal and intraretinal compartments, leading to permanent barrier loss and PCRD development. OCT = optical coherence tomography; ORE = outer retinal erosion; ORP = outer retinal pinching.

in CSCR: ORE and ORP. They seem to be correlated with different pathophysiological aspects regarding the amount and content of the leaking fluid. Our observations suggest that these patterns remain independent over time and can represent a foundation for possible different trajectories in the disease progression.

In ORE, the external segments of photoreceptors undergo a focal process of erosion⁷ along an otherwise thickened outer photoreceptor layer. This local loss of stacked discs of photoreceptors, which we defined as “tooth loss sign,” is likely produced by the mechanical insult of fluid flow coming from the RPE defect on the opposite side. The erosion can be a limited notch or a broader defect, depending on the leakage duration and recurrence. In any case, it is different from the larger and poorly demarcated attenuation of the outer retina, with possible foveal atrophy, resulting from the chronic persistence of SRF. In our follow-up window, no case developed foveal atrophy because of the limited persistence of the serous retinal detachment after spontaneous resolution or PDT.

Conversely, ORP is characterized by a focal adherence between the outer retina and the RPE within the macular detachment. This scenario is typical of CSCR with fibrinous exudation, profuse leakage intensity, and high volume of SRF. In all instances, a more or less detectable bridge of hyperreflective material connects the RPE plane with the outer retinal surface, creating a characteristic “pinching” effect on both sides, often better appreciable on the retinal side. Even when hyperreflective material is not distinctly visualized, the presence of focal pinching suggests subclinical fibrin deposits are responsible for the mechanical adherence between outer retina and RPE.

The typical presentation of CSCR, as depicted in textbook images and prevalent in medical imaging databases, characteristically displays SRF with a triangular configuration on B-scan OCT. These geometric characteristics have engendered significant scientific interest, with researchers focusing on various morphological parameters, including the angle formed between the SRF apex and its lateral legs (“Fuji Sign”³⁵), as well as height-to-width ratios that serve as surrogate markers for differentiation between flatter and more dome-shaped SRF morphologies.³⁶ Three-dimensional rendering of serous retinal detachment configuration has been investigated primarily in relation to spontaneous resolution patterns or gravitational inferior shifting of fluid.³⁷

In the present study, we used external AI-based software to provide enhanced quantification of SRF and PED volumes and developed an internal algorithm to visualize the 3-dimensional configuration of macular detachment. We observed a significant association of ORP with greater volumes of SRF and PED independently by the presence of unifocal or multifocal leaks (Table 2). In relation to the shape of the macular detachment, cases with ORE were characterized by the conventional dome shape with a more or less pronounced peak corresponding to the photoreceptor ero-

sion site, whereas cases with ORP had a toroidal configuration (Figure 2). In the latter, the distinctive morphology facilitates the identification and topographic localization of the critical zone of SRF origin and the site of a potential communication between the choroid and intraretinal compartments. The evolution toward PCRD only seen in cases with these characteristics suggests that the focal area of ORP, once an adherent atrophic-fibrous scar has established, constitutes a site of lack of barriers (RPE and retinal external limiting membrane) that allows direct passage of fluid from the interstitial choroidal tissue into the retina.

Our analysis revealed that the presence of a fibrin bridge between the RPE and the outer photoreceptor layer was the predominant finding associated with ORP, observed in 86.3% of cases. Conversely, subretinal fibrin was not detected in any ORE case, resulting in a key distinguishing feature between the two groups. Even in the 6 of 44 eyes with ORP in which subretinal hyperreflective material was not distinctly visualized on OCT, we can infer the presence of fibrin because there was a focal contact and bilateral traction between the outer retinal surface and the RPE (“clepsydra sign”), which is reasonably due to the strong adhesive properties of the fibrin proteins. Therefore, subretinal fibrin^{13,17,29,39-41} (also defined in the reference literature as white subretinal exudation,^{42,43} fibrinous or fibrin-like subretinal hyperreflective material^{38,44-47}) is a crucial OCT biomarker in the proposed classification scheme. Additionally, hyporefective lucency^{19,48,49} (also previously defined as translucent shadow,¹³ “vacuole sign,”⁵⁰ pellucid core,⁴⁵ or “dark spot”^{42,51-53} within subretinal fibrin) was present in a subset of patients within well-defined and large fibrin deposits on the plane of the RPE. Our observations confirm, as already proposed, that the hyporefective lucency is associated with profound subretinal exudation and represents a specific biomarker for localization of the leaking site.⁴⁴

The presence of fibrinous exudate in the subretinal space of patients with CSCR has been demonstrated histologically in both human specimens⁵⁴ and experimental intravenous adrenaline-induced primate models of CSCR,⁵⁵ and carries significant pathophysiological implications. It indicates a particularly marked increase of choroidal vascular permeability associated with wide breakdown of the outer blood-retinal barrier. Such permeability must be sufficient to permit extravasation of large fibrinogen molecules (340 kDa) across the compromised choriocapillaris endothelium and the RPE. These considerations align with our quantitative findings of significantly greater SRF and PED volumes (Figure 4), and clinical association of atypically profuse leaks (Table 2) in ORP cases compared with ORE cases.

In cases with multifocal leaks, all leaks in the same eye, also if numerous, were associated with the same subretinal pattern, ORE or ORP. This suggests a different pathophysiological basis of the exudative process for the ORE and ORP cases. Our findings also revealed that ORP cases were significantly more often steroid related than ORE cases (40.9% vs 18.6%, $P = .011$), strengthening the need for a careful

investigation of possible exposure to steroids in the clinical history of these patients. This observation aligns with reports by Uyama and associates⁵⁶ linking corticosteroid administration to severe exudative forms of CSCR and with the experimental observation of inhibition of RPE repair processes by steroids.⁵⁷

The evidence of subretinal pinching and fibrin, indicating pronounced choroidal permeability, should additionally put on notice for a possible exaggerated response to PDT due to excessive accumulation of verteporfin in the exudation area. This heightened response can potentially lead to or accelerate a chorioretinal adhesive scarring, which further promotes intraretinal changes. In the 2 cases where development of PCRD was observed just after PDT, this mechanism could be called into question. A potential exaggerated response of fibrinous chorioretinal lesions to PDT was first reported by Yannuzzi,⁵⁸ who noted the biochemical similarity between verteporfin and ICG molecules in their ability to bind to fibrin. Subsequent reports by Liang and associates⁵⁹ have indicated a higher safety profile for half-dose versus full-dose PDT in cases with documented subretinal fibrin deposition, suggesting that lower treatment parameters may mitigate risks while maintaining therapeutic efficacy.

Ultimately, in CSCR with ORP, the management of the disease can be more difficult than in cases with ORE because the frequent presence of steroid intake as a risk factor leads to taking its suspension as the first therapeutic measure, postponing other treatments. Furthermore, the presence of fibrin makes one hesitant in the decision to undergo PDT, leading to proceed with longer periods of observation. This behavior may have played a role in the evolution toward PCRD and uncontrolled exudation in our 5 untreated ORP cases that developed PCRD with a median time to event of 7.5 months (IQR, 6.3-12.5).

Nonvasogenic infiltration of fluid into the retina at the posterior pole, defined as PCRD, is considered to be an end-stage manifestation of CSCR implying a condition of advanced permanent breakdown of the outer blood-retinal barrier and dysfunctionality of the retinal external limiting membrane.^{9,10,60} Therefore, there has been sustained interest in understanding the mechanisms of IRF formation in CSCR.⁶¹ In a previous study focusing on cases with established PCRD,¹¹ the presence of patches/bands of subretinal fibrosis was significantly associated with cystoid degeneration, suggesting that adherence between the choroid and retina could facilitate fluid passage from the choroid to the intraretinal space. Once a direct communication between choroid and retina is established, intraretinal cysts become highly responsive to changes in their differential pressure with the interstitial choroidal compartment. This phenomenon was clinically demonstrated in a case of CSCR with stable PCRD where ocular contusion induced choroidal congestion and rapid exacerbation of the cystoid lesion volume.⁶² Furthermore, the recent recognition of a significant role of low intraocular pressure and high

ocular perfusion pressure in the pathophysiology of CSCR² suggests that hemodynamic parameters may also influence the amount of the intraretinal fluid in CSCR with established PCRD.

The current study enriches PCRD description by capturing the transition between the initial leak causing SRF accumulation and the subsequent development of IRF in primary and recurrent CSCR phenotypes, thereby providing insight into the early pathophysiological mechanisms that precede permanent retinal cystoid changes. Our time-to-event analysis demonstrated a dichotomy in disease progression between the two initial morphological patterns because this transition occurred exclusively in ORP cases. Interestingly, all cases that developed PCRD (Table 4) presented with blot-type leakage, recurrent episodes, and the presence of subretinal fibrin, with hyporeflective lucency evident in a subset of 2 of 7 cases, with a median time to IRF development of 7.5 months from baseline (IQR, 6.1-9.8 months). Therefore, the PCRD complication does not seem due to the chronicity of serous detachment, but rather it seems to strictly correlate with the establishment of a communication between the choroidal and retinal interstitial spaces through an adherent chorioretinal lesion where the integrity of the RPE barrier is compromised.^{63,64} Our extended follow-up data demonstrate that although PDT treatment in PCRD cases secondary to ORP may show initial suboptimal responses with incomplete resolution, appropriate therapeutic management can mitigate the visual impact of this complication.

Foveal atrophy did not develop in any case in this study. This severe macular damage is the consequence of a longstanding persistence of SRF in the central macula and is associated with severe visual loss.^{65,66} The overall favorable anatomic and visual outcome of ORE cases (Figure 8) observed in our follow-up cohort demonstrates that CSCR with this finding, when diagnosed early and managed appropriately, can be considered a non-vision-threatening condition in which visual function can be entirely preserved. An equally good anatomic prognosis is not a given for all cases of CSCR seen in early stages when ORP is present, despite the adequacy of the therapeutic management and follow-up that can be provided. The potential for PCRD development should be carefully considered in these cases, as well as the potential risk of an exaggerated response to PDT for the presence of fibrin. In these patients, alternative treatments should be considered. Nevertheless, PCRD development appears to occur in only a limited subset of patients with ORP and does not seem to result in severe visual loss.

Of note, our study underlines the strong spatial correlation between fluorescein angiographic leaks and early structural outer retinal alterations. In early cases of CSCR, ORE and ORP findings could serve as reliable biomarkers for identifying treatment targets, potentially reducing the need for invasive angiographic procedures in the management of CSCR. Moreover, the presence of high-volume SRF should

prompt clinicians to suspect an ORP leak pattern and guide a thorough examination of the entire SRF extent to identify the critical area of fluid origin and possible fibrin deposition. On the other side, when we decide to apply PDT in cases of chronic CSCR with intraretinal and subretinal exudation, the chorioretinal adherence and cyst topography can be used as late biomarkers to identify the site of origin of fluid without resorting to invasive methods.

Regarding the limitations of the study, we acknowledge that our results on SRF volumes may be affected by the timing of presentation of the active episode, even if it was less than 4 months for all cases. Other limitations of this study include its nonconcurrent nature, the relatively small number of patients with longitudinal data, and the variable follow-up durations, making long-term outcomes difficult to assess uniformly across all patients. The exclusive occurrence of PCRD in the ORP group precluded the application of proportional hazards modeling to quantify adjusted risk estimates due to the complete outcome separation. Larger studies are needed to confirm our results and to discern the prognostic value of ORE and ORP patterns with reference to the possible advanced anatomic and functional outcomes in CSCR.

In conclusion, our study delineates a two-pattern classification of early morphological changes in CSCR: ORE and ORP. They reflect fundamentally distinct pathophysiologic conditions that produce a different quantity and quality of leaking fluid, and predispose to divergent disease trajectories. Specifically, ORP cases, marked by higher SRF volumes and fibrinous exudation, exclusively seem to be able

to develop PCRD in a medium-term follow-up, despite PDT treatment or maybe even as a consequence of it. ORE and ORP detected by OCT in early active cases of CSCR may be considered as signature biomarkers of the site of RPE leakage and used as a guide for treatment planning without invasive examinations.

CREDIT AUTHORSHIP CONTRIBUTION STATEMENT

Paolo Forte: Writing – review & editing, Writing – original draft, Visualization, Investigation, Formal analysis, Data curation, Conceptualization. **Jennifer Cattaneo:** Writing – original draft, Methodology, Investigation, Data curation. **Su-chun Huang:** Writing – original draft, Visualization, Software, Methodology, Formal analysis, Data curation. **Paolo Corazza:** Supervision, Investigation, Data curation. **Simon Magnin:** Investigation, Data curation. **Lorenzo Mangoni:** Supervision. **Stefano Ranno:** Supervision. **Christian Cordano:** Validation, Supervision. **Antonio Polito:** Supervision, Data curation. **Massimo Nicolò:** Supervision. **Michele Iester:** Validation, Supervision. **Marco Lupidi:** Writing – review & editing, Validation, Supervision. **Chiara Maria Eandi:** Writing – review & editing, Validation, Supervision, Methodology, Investigation, Conceptualization. **Felice Cardillo Piccolino:** Writing – review & editing, Writing – original draft, Supervision, Methodology, Conceptualization.

Funding/Support: This work was supported by Fondazione Ferrero, Alba, Italy and Fondazione Italiana Macula ETS, Genova, Italy. **Financial Disclosures:** The authors indicate no financial support or conflicts of interest. All authors attest that they meet the current ICMJE criteria for authorship. Deidentified datasets generated/analyzed in the present study will be available upon reasonable request to the corresponding author. **Author Contributions:** Conceptualization, Investigation, Data curation, Writing – Original Draft, Review and Editing: P.F. Investigation, Data curation, Writing – original draft: J.C. Formal analysis, Data curation, Writing – Original Draft: S.H. Investigation, Data curation: P.C. Investigation, Data curation: S.M. Supervision: L.M. Supervision: S.R. Supervision: C.C. Investigation: A.P. Supervision: M.N. Methodology, Supervision: M.I. Methodology, Supervision: M.L. Conceptualization, Writing – Review & Editing, Supervision: C.M.E. Conceptualization, Methodology, Writing – Review & Editing, Supervision: F.C.P.

REFERENCES

1. Gass JD. Pathogenesis of disciform detachment of the neuroepithelium. *Am J Ophthalmol.* 1967;63(3):1–139.
2. Cardillo Piccolino F, Arrigo A, Forte P, et al. Intraocular pressure and ocular perfusion pressure in central serous chorioretinopathy. *Am J Ophthalmol.* 2025 Published online August 22S0002-9394(25)00458-1. doi:10.1016/j.ajo.2025.08.045.
3. Ramtohul P, Cabral D, Oh D, Galhoz D, Freund KB. En face ultrawidefield oct of the vortex vein system in central serous chorioretinopathy. *Ophthalmol Retina.* 2023;7(4):346–353. doi:10.1016/j.oret.2022.10.001.
4. Forte P, Cattaneo J, Cardillo Piccolino F, et al. Influence of scleral thickness on photodynamic therapy outcomes in central serous chorioretinopathy. *Acta Ophthalmol.* 2025;103(3):e165–e175. doi:10.1111/aos.16779.
5. Koizumi H, Imanaga N, Terao N. Central serous chorioretinopathy and the sclera: what we have learned so far. *Jpn J Ophthalmol.* 2024;68(5):419–428. doi:10.1007/s10384-024-01101-2.
6. Forte P, Feo A, Koizumi H, et al. Scleral thickness in eyes with pachychoroid pigment epitheliopathy accompanied by keratoconus. *Ophthalmol Sci.* 2025;5(5):100808. doi:10.1016/j.xops.2025.100808.
7. Cardillo Piccolino F, de la Longrais RR, Ravera G, et al. The foveal photoreceptor layer and visual acuity loss in central serous chorioretinopathy. *Am J Ophthalmol.* 2005;139(1):87–99. doi:10.1016/j.ajo.2004.08.037.
8. Eandi CM, Chung JE, Cardillo Piccolino F, Spaide RF. Optical coherence tomography in unilateral resolved central serous chorioretinopathy. *Retina.* 2005;25(4):417–421. doi:10.1097/00006982-200506000-00004.
9. Iida T, Yannuzzi LA, Spaide RF, Borodoker N, Carvalho CA, Negro S. Cystoid macular degeneration in chronic central serous chorioretinopathy. *Retina.* 2003;23(1):1–7 quiz 137–138. doi:10.1097/00006982-200302000-00001.

10. Cardillo Piccolino F, De La Longrais RR, Manea M, Cicinelli S. Posterior cystoid retinal degeneration in central serous chorioretinopathy. *Retina*. 2008;28(7):1008–1012. doi:10.1097/IAE.0b013e31816b4b86.
11. Cardillo Piccolino F, De La Longrais RR, Manea M, Cicinelli S, Ravera G. Risk factors for posterior cystoid retinal degeneration in central serous chorioretinopathy. *Retina*. 2008;28(8):1146–1150. doi:10.1097/IAE.0b013e318175421f.
12. Mohabati D, Hoyng CB, Yzer S, Boon CJF. Clinical characteristics and outcome of posterior cystoid macular degeneration in chronic central serous chorioretinopathy. *Retina*. 2020;40(9):1742–1750. doi:10.1097/IAE.0000000000002683.
13. Fujimoto H, Gomi F, Wakabayashi T, Sawa M, Tsujikawa M, Tano Y. Morphologic changes in acute central serous chorioretinopathy evaluated by Fourier-domain optical coherence tomography. *Ophthalmology*. 2008;115(9):1494–1500.e1-2. doi:10.1016/j.ophtha.2008.01.021.
14. Daruich A, Matet A, Dirani A, et al. Central serous chorioretinopathy: recent findings and new physiopathology hypothesis. *Prog Retin Eye Res*. 2015;48:82–118. doi:10.1016/j.preteyeres.2015.05.003.
15. Maltsev DS, Kulikov AN, Chhablani J. Topography-guided identification of leakage point in central serous chorioretinopathy: a base for fluorescein angiography-free focal laser photocoagulation. *Br J Ophthalmol*. 2018;102(9):1218–1225. doi:10.1136/bjophthalmol-2017-311338.
16. Song IS, Shin YU, Lee BR. Time-periodic characteristics in the morphology of idiopathic central serous chorioretinopathy evaluated by volume scan using spectral-domain optical coherence tomography. *Am J Ophthalmol*. 2012;154(2):366–375. doi:10.1016/j.ajo.2012.02.031.
17. Kim HC, Cho WB, Chung H. Morphologic changes in acute central serous chorioretinopathy using spectral domain optical coherence tomography. *Korean J Ophthalmol*. 2012;26(5):347–354. doi:10.3341/kjo.2012.26.5.347.
18. Yu J, Jiang C, Xu G. Study of subretinal exudation and consequent changes in acute central serous chorioretinopathy by optical coherence tomography. *Am J Ophthalmol*. 2014;158(4):752–756. doi:10.1016/j.ajo.2014.06.015.
19. Yannuzzi NA, Mrejen S, Capuano V, Bhavsar KV, Querques G, Freund KB. A central hyporeflective subretinal lucency correlates with a region of focal leakage on fluorescein angiography in eyes with central serous chorioretinopathy. *Ophthalmic Surg Lasers Imaging Retina*. 2015;46(8):832–836. doi:10.3928/23258160-20150909-07.
20. Nicolás M, Eandi CM, Alovisei C, et al. Half-fluence versus half-dose photodynamic therapy in chronic central serous chorioretinopathy. *Am J Ophthalmol*. 2014;157(5):1033–1037. doi:10.1016/j.ajo.2014.01.022.
21. Chhablani J, Cohen FBCentral Serous Chorioretinopathy International Group. Multimodal imaging-based central serous chorioretinopathy classification. *Ophthalmol Retina*. 2020;4(11):1043–1046. doi:10.1016/j.oret.2020.07.026.
22. Cheung CMG, Dansingani KK, Koizumi H, et al. Pachychoroid disease: review and update. *Eye (Lond)*. 2025;39(5):819–834. doi:10.1038/s41433-024-03253-4.
23. Cardillo Piccolino F, Borgia L, Zinicola E, Zingirian M. Indocyanine green angiographic findings in central serous chorioretinopathy. *Eye (Lond)*. 1995;9(Pt 3):324–332. doi:10.1038/eye.1995.63.
24. Dansingani KK, Balaratnasingam C, Mrejen S, et al. Annular lesions and catenary forms in chronic central serous chorioretinopathy. *Am J Ophthalmol*. 2016;166:60–67. doi:10.1016/j.ajo.2016.03.025.
25. Lupidi M, Fruttini D, Eandi CM, et al. Chronic neovascular central serous chorioretinopathy: a stress/rest optical coherence tomography angiography study. *Am J Ophthalmol*. 2020;211:63–75. doi:10.1016/j.ajo.2019.10.033.
26. Wang MSM, Sander B, Larsen M. Retinal atrophy in idiopathic central serous chorioretinopathy. *Am J Ophthalmol*. 2002;133(6):787–793. doi:10.1016/s0002-9394(02)01438-1.
27. Schatz H, Burton TC, Yannuzzi LA, Rabb MF. *Choroidal leaks, Interpretation of Fundus Fluorescein Angiography C.V. Mosby Co; 1978:644–653.*
28. Kogo T, Muraoka Y, Ishikura M, et al. Pigment epithelial detachment and leak point locations in central serous chorioretinopathy. *Am J Ophthalmol*. 2024;261:19–27. doi:10.1016/j.ajo.2024.01.012.
29. Shukla D, Aiello LP, Kolluru C, Baddela S, Jager RD, Kim R. Relation of optical coherence tomography and unusual angiographic leakage patterns in central serous chorioretinopathy. *Eye (Lond)*. 2008;22(4):592–596. doi:10.1038/sj.eye.6702818.
30. Kurmann T, Yu S, Márquez-Neila P, et al. Expert-level automated biomarker identification in optical coherence tomography scans. *Sci Rep*. 2019;9(1):13605. doi:10.1038/s41598-019-49740-7.
31. Ferro Desideri L, Anguita R, Berger LE, et al. Baseline spectral domain optical coherence tomographic retinal layer features identified by artificial intelligence predict the course of central serous chorioretinopathy. *Retina*. 2024;44(2):316–323. doi:10.1097/IAE.0000000000003965.
32. Cattaneo J, Forte P, Forte G, Eandi CM. Faricimab efficacy in type 1 macular neovascularization: AI-assisted quantification of pigment epithelium detachment (PED) volume reduction over 12 months in Naïve and switch eyes. *Int J Retina Vitreous*. 2025;11(1):3. doi:10.1186/s40942-025-00629-w.
33. Cardillo Piccolino F. Laser treatment of eccentric leaks in central serous chorioretinopathy resulting in disappearance of untreated juxtafoveal leaks. *Retina*. 1992;12(2):96–102. doi:10.1097/00006982-199212020-00004.
34. Eandi CM, Ober M, Iranmanesh R, Peiretti E, Yannuzzi LA. Acute central serous chorioretinopathy and fundus autofluorescence. *Retina*. 2005;25(8):989–993. doi:10.1097/00006982-200512000-00006.
35. Feenstra HMA, Hensman J, Gkika T, et al. Spontaneous resolution of chronic central serous chorioretinopathy: “Fuji Sign”. *Ophthalmol Retina*. 2022;6(9):861–863. doi:10.1016/j.oret.2022.04.023.
36. Subhi Y, Bjerager J, Boon CJF, van Dijk EHC. Subretinal fluid morphology in chronic central serous chorioretinopathy and its relationship to treatment: a retrospective analysis on PLACE trial data. *Acta Ophthalmol*. 2022;100(1):89–95. doi:10.1111/aos.14901.
37. Ahn SE, Oh J, Oh JH, Oh IK, Kim SW, Huh K. Three-dimensional configuration of subretinal fluid in central serous chorioretinopathy. *Invest Ophthalmol Vis Sci*. 2013;54(9):5944–5952. doi:10.1167/iovs.13-12279.

38. Sahoo NK, Govindhari V, Bedi R, et al. Subretinal hyperreflective material in central serous chorioretinopathy. *Indian J Ophthalmol.* 2020;68(1):126–129. doi:10.4103/ijo.IJO_265_19.
39. Schatz H, McDonald HR, Johnson RN, et al. Subretinal fibrosis in central serous chorioretinopathy. *Ophthalmology.* 1995;102(7):1077–1088. doi:10.1016/s0161-6420(95)30908-6.
40. Hussain N, Baskar A, Ram LM, Das T. Optical coherence tomographic pattern of fluorescein angiographic leakage site in acute central serous chorioretinopathy. *Clin Exp Ophthalmol.* 2006;34(2):137–140. doi:10.1111/j.1442-9071.2006.01171.x.
41. Saxena S, Sinha N, Sharma S. Three-dimensional imaging by spectral domain optical coherence tomography in central serous chorioretinopathy with fibrin. *J Ocul Biol Dis Infor.* 2011;4(4):149–153. doi:10.1007/s12177-012-9087-9.
42. Gass JD. Central serous chorioretinopathy and white subretinal exudation during pregnancy. *Arch Ophthalmol.* 1991;109(5):677–681. doi:10.1001/archoph.1991.01080050091036.
43. Ie D, Yannuzzi LA, Spaide RF, Rabb MF, Blair NP, Daily MJ. Subretinal exudative deposits in central serous chorioretinopathy. *Br J Ophthalmol.* 1993;77(6):349–353.
44. Funatsu R, Terasaki H, Mihara N, et al. Identification of leakage sites in central serous chorioretinopathy using optical coherence tomography and the assessment of the characteristics of the biomarkers. *Retina.* 2025;45(5):893–900. doi:10.1097/IAE.0000000000004404.
45. Pu J, He G, Zhang X, et al. Multimodal imaging biomarkers of subretinal hyperreflective material accumulation in central serous chorioretinopathy. *Photodiagnosis Photodyn Ther.* 2025;53:104595. doi:10.1016/j.pdpdt.2025.104595.
46. Feo A, Stradiotto E, Sacconi R, Menean M, Querques G, Romano MR. Subretinal hyperreflective material in retinal and chorioretinal disorders: a comprehensive review. *Surv Ophthalmol.* 2024;69(3):362–377. doi:10.1016/j.survophthal.2023.10.013.
47. Shinjima A, Hirose T, Mori R, Kawamura A, Yuzawa M. Morphologic findings in acute central serous chorioretinopathy using spectral domain-optical coherence tomography with simultaneous angiography. *Retina.* 2010;30(2):193–202. doi:10.1097/IAE.0b013e3181c70203.
48. Fossataro F, Fossataro C, Abraham N, et al. Pathogenesis of central serous chorioretinopathy and the link between choroidal hyperpermeability and retinal pigment epithelium pump reversal. *Am J Ophthalmol.* 2024;266:206–217. doi:10.1016/j.ajo.2024.04.025.
49. Bijon J, Freund KB. Hyporeflective subretinal lucency in central serous chorioretinopathy. *Ophthalmology.* 2024;131(12):1481. doi:10.1016/j.ophtha.2023.12.023.
50. Rajesh B, Kaur A, Giridhar A, Gopalakrishnan M. Vacuole” sign adjacent to retinal pigment epithelial defects on spectral domain optical coherence tomography in central serous chorioretinopathy associated with subretinal fibrin. *Retina.* 2017;37(2):316–324. doi:10.1097/IAE.0000000000001192.
51. Parchand S, Gupta V, Gupta A, Dogra MR, Singh R, Sharma A. Dark spot in fibrinous central serous chorioretinopathy masquerading choroiditis. *Ocul Immunol Inflamm.* 2013;21(3):201–206. doi:10.3109/09273948.2013.765015.
52. Otsuka S, Ohba N, Nakao K. A long-term follow-up study of severe variant of central serous chorioretinopathy. *Retina.* 2002;22(1):25–32. doi:10.1097/00006982-200202000-00005.
53. Singh SR, Dogra M, Dogra MR. Dark spot in fibrinous central serous chorioretinopathy. *JAMA Ophthalmol.* 2018;136(10):e182924. doi:10.1001/jamaophthalmol.2018.2924.
54. deVenecia G. Fluorescein angiographic smoke stack. Case presentation at Verhoeff Society Meeting; April 24–25, 1982; Washington, DC. *Stereoscopic Atlas of Macular Diseases.* St Louis: CV Mosby Co.; 1987:46–59.
55. Yoshioka H, Katsume Y. Experimental central serous chorioretinopathy. III: ultrastructural findings. *Jpn J Ophthalmol.* 1982;26(4):397–409.
56. Uyama M, Matsunaga H, Matsubara T, et al. Indocyanine green angiography in multifocal posterior pigment epitheliopathy. In: Coscas G, Cardillo Piccolino F, eds. *Retinal Pigment Epithelium and Macular Diseases.* Netherlands: Springer; 1998:255–262. doi:10.1007/978-94-011-5137-5_42.
57. Kishimoto N, Uyama M, Fukushima I, Yamada K, Nishikawa M, Ohkuma H. [The effect of corticosteroid on the repair of the retinal pigment epithelium]. *Nippon Ganka Gakkai Zasshi.* 1993;97(3):360–369.
58. Yannuzzi LA. Central serous chorioretinopathy: a personal perspective. *Am J Ophthalmol.* 2010;149(3):361–363. doi:10.1016/j.ajo.2009.11.017.
59. Liang Z, Qu J, Huang L, et al. Comparison of the outcomes of photodynamic therapy for central serous chorioretinopathy with or without subfoveal fibrin. *Eye (Lond).* 2021;35(2):418–424. doi:10.1038/s41433-020-0858-4.
60. Gaudric A, Audo I, Vignal C, et al. Non-vasogenic cystoid maculopathies. *Prog Retin Eye Res.* 2022;91:101092. doi:10.1016/j.preteyeres.2022.101092.
61. Astroz P, Balaratnasingam C, Yannuzzi LA. Cystoid macular edema and cystoid macular degeneration as a result of multiple pathogenic factors in the setting of central serous chorioretinopathy. *Retin Cases Brief Rep.* 2017;11(Suppl 1):S197–S201. doi:10.1097/ICB.0000000000000443.
62. Cardillo Piccolino F. Effect of ocular contusion in a patient with chronic central serous chorioretinopathy. *Retin Cases Brief Rep.* 2010;4(1):47–50. doi:10.1097/ICB.0b013e318196b206.
63. Kumar Sahoo N, Lupidi M, Goud A, Gangakhedkar S, Cardillo Piccolino F, Chhablani J. One-year outcome of cystoid macular degeneration in central serous chorioretinopathy. *Eur J Ophthalmol.* 2022;32(4):2347–2354. doi:10.1177/11206721211046497.
64. Fukuyama H, Komuku Y, Gomi F. Characteristics and treatment responses of cystoid retina associated with central serous chorioretinopathy. *Jpn J Ophthalmol.* 2021;65(3):372–379. doi:10.1007/s10384-021-00815-x.
65. Son KY, Lim SG, Hwang S, Choi J, Kim SJ, Kang SW. Foveal atrophy in patients with active central serous chorioretinopathy at first presentation: characteristics and treatment outcomes. *Br J Ophthalmol.* 2024;109(1):89–97. doi:10.1136/bjo-2023-324147.
66. Hasan N, Zarnegar A, Jacob N, et al. Clinical characteristics and progression of pachychoroid macular atrophy in central serous chorioretinopathy. *Ophthalmol Retina.* 2025;9(10):984–993. doi:10.1016/j.oret.2025.04.005.